Facile hydrothermal synthesis of ultra-long manganese oxyhydroxide nanorods and their transformation into MnO_2 and Mn_2O_3 nanorods

Zhong Chun Li, Si Si Chen, Chao Dong, Xu Hong Chen, Quan Fa Zhou

School of Chemistry and Environment Engineering, Jiangsu University of Technology, Changzhou 213001, People's Republic of China
E-mail: czlizc@126.com

Published in Micro & Nano Letters; Received on 12th January 2013; Revised on 9th May 2013; Accepted on 14th May 2013

Single-crystal manganese oxyhydroxide (MnOOH) nanorods with high aspect ratios have been successfully prepared employing a simple hydrothermal route based on the redox between potassium permanganate ($KMnO_4$) and polyvinyl pyrrolidone (PVP). By adjusting the reaction temperature, reaction time and the mass ratio of PVP/$KMnO_4$, MnOOH nanorods with lengths up to 20 μm and diameters in the range of 100–400 nm could be facilely prepared in high yield. The as-prepared MnOOH nanorods were characterised by X-ray diffraction, scanning electron microscopy, transmission electron microscopy, high-resolution transmission electron microscopy and Fourier transformed infrared spectroscopy. The formation mechanism of MnOOH nanorods was preliminarily discussed based on the Ostwald's ripening process. Furthermore, MnO_2 and Mn_2O_3 nanorods with high aspect ratios were synthesised by calcination of MnOOH nanorods.

1. Introduction: Manganese-based nanostructures have attracted tremendous attention because of their outstanding structural diversity [1], physical and chemical properties [2] and potential applications in many fields such as sensors [3], catalysts [4], batteries [5] and supercapacitors [6]. Many approaches including solvothermal or hydrothermal routes [7], the sol–gel technique [8], electrochemical deposition [9], ultrasonic [10], thermal decomposition [11], vapour phase growth [12], gamma or microwave irradiation [13] and the chemical precipitation method [14], have been developed for synthesis of various manganese-based nanostructures. Although much effort has been made and some successes have been achieved, the synthesis of manganese-based nanostructures with controllable phase, morphology and size, especially the preparation of one-dimensional manganese-based nanostructures in a controlled way, remains a big challenge [15]. Among the manganese-based compounds, manganese oxyhydroxide (MnOOH) has attracted a great deal of attention because of its potential applications in many fields such as catalysis [16] and supercapacitors [17]. Meanwhile, it can be readily transformed into several different manganese oxides, such as Mn_3O_4 [18], MnO_2 and Mn_2O_3, which have been extensively used as catalysts and electrode materials [19–22]. In this Letter, we report a simple hydrothermal route to synthesis of MnOOH nanorods under mild conditions based on the redox between potassium permanganate ($KMnO_4$) and polyvinyl pyrrolidone (PVP). MnOOH nanorods with high aspect ratios were achieved by simply tuning the mass ratio of PVP/$KMnO_4$, reaction temperature and reaction time. Furthermore, uniform MnO_2 nanorods were synthesised by calcination of MnOOH nanorods at 300°C. Also, Mn_2O_3 nanorods were obtained at 400 or 600°C.

2. Experimental

2.1. Materials: $KMnO_4$ and PVP (K-30) were purchased from the Sinopharm Chemical Reagent Co. Ltd. The water used throughout the experiments was thrice-distilled water.

2.2. Synthesis of MnOOH nanorods: A suitable amount of PVP was dissolved in 15.0 ml of thrice-distilled water, and then 0.20 g $KMnO_4$ was added into the above solution. After stirring vigorously, the resultant solution was transferred to a 25 ml Teflon-lined pressure vessel, stainless steel autoclave. The autoclave was sealed and heated in an oven at a given temperature for different times. The pressure vessel was allowed to cool to room temperature naturally. The precipitate was collected by centrifugation and washed with water and ethanol several times, then the precipitate was dried in air.

2.3. Calcination preparation of MnO_2 and Mn_2O_3 nanorods: MnO_2 and Mn_2O_3 nanorods were prepared from MnOOH nanorods. MnOOH nanorods were put into a crucible. The crucible was then transferred into a muffle furnace. The temperature of the muffle furnace was raised to the designated temperature and maintained at this temperature for 10 h. Finally, the black powder was collected.

2.4. Characterisation: X-ray diffraction (XRD) analyses were performed on a Bruker D8 advance diffractometer with Cu $K\alpha$ radiation ($\lambda = 0.15406$ nm). Scanning electron microscopy (SEM) images were obtained with HITACHI-3400s and HITACHI-4800. TEM images were observed on a Tecnai-12 transmission electron microscope (TEM) operating at 120 kV. High-resolution transmission electron microscopy (HRTEM) characterisation was performed with an FEI Tecnai G2 F30 S-TWIN field-emission TEM operating at 300 kV. A Fourier transformed infrared spectroscopy (FTIR) spectrum was obtained using a Nicolet 200 model Fourier transformed infrared spectrometer.

3. Results and discussion

3.1. XRD analyses of MnOOH nanorods: The structure of as-prepared MnOOH nanorods was determined by XRD. A typical XRD pattern of MnOOH nanorods is shown in Fig. 1. It can be seen that the MnOOH nanorods were well crystallised. All of the reflections in Fig. 1 can be attributed to a monoclinic phase of MnOOH with lattice constants $a = 5.304$ Å, $b = 5.277$ Å, $c = 5.304$ Å, compatible with literature values (JCPDS No. 88-0649) [23]. The XRD result preliminarily indicates that high purity MnOOH nanorods could be synthesised through the redox between $KMnO_4$ and PVP.

3.2. Microstructure and morphology of MnOOH nanorods: The morphologies of the resulting samples were investigated by SEM and TEM. Fig. 2*a* shows a typical SEM image of MnOOH nanorods. The overall morphology of the sample is shown in

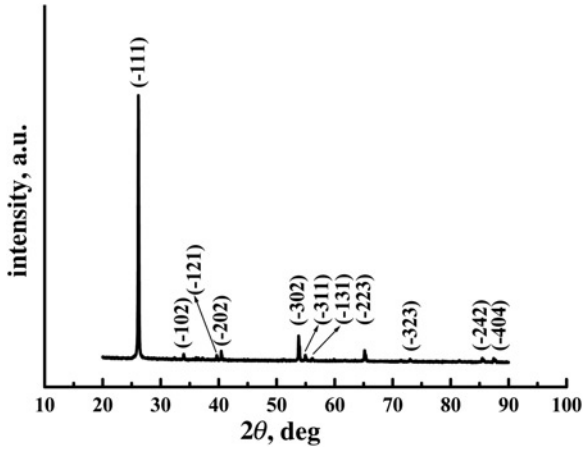

Figure 1 *XRD pattern of MnOOH nanorods*

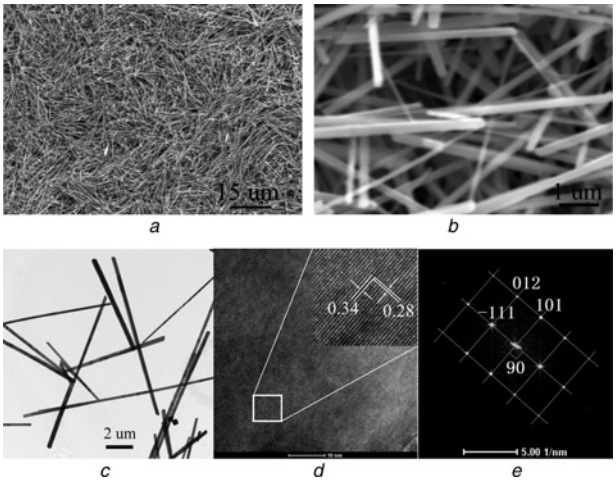

Figure 2 *SEM, TEM and HRTEM, and corresponding FFT pattern, of MnOOH nanorods synthesised at 160°C for 16 h with the mass ratio between PVP and $KMnO_4$ of 2.0*
a SEM image
b Image with higher magnification
c TEM image
d HRTEM image
e Corresponding FFT pattern

Fig. 2*a*. Fig. 2*b* shows the morphology of the sample with higher magnification, which indicates that the sample is composed of a large quantity of MnOOH nanorods. It is interestingly observed that these MnOOH nanorods have cross-sections of tetragonal shape. Fig. 2*c* shows a typical TEM image of MnOOH nanorods. As shown in Fig. 2*c*, MnOOH nanorods with high aspect ratios were obtained. The TEM image shows that the diameter is 100 – 400 nm and the average length is about 10 – 15 μm. HRTEM was used to characterise further the crystal structure of individual MnOOH nanorods. Fig. 2*d* provides a representative HRTEM image of an MnOOH nanorod. The HRTEM image shows many lattice planes with perfect crystallinity. The inset in Fig. 2*d* shows the enlarged view of the square region to identify the lattice planes forming this MnOOH nanorod. The interplanar distances of 0.34 and 0.28 nm correspond to the (−111) and (101) planes of a monoclinic phase of MnOOH. Fig. 2*e* presents the corresponding fast-Fourier transform (FFT) pattern. The FFT pattern indicates the MnOOH nanorod is single crystal in nature. Calculations indicate that the angle between the (−111) and (101) planes is 90°, which is consistent with the results of HRTEM and FFT patterns.

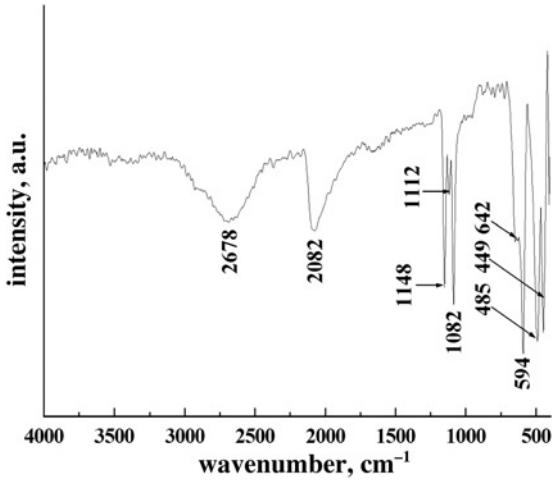

Figure 3 *FTIR spectrum of MnOOH nanorods*

3.3. FTIR spectrum analysis: The FTIR spectrum of MnOOH nanorods is shown in Fig. 3. In the 400–4000 cm^{-1} range, the sharp peaks at 449, 485, 594 and 642 cm^{-1} are attributed to the vibrations of the Mn–O bonds in MnOOH [24]. The peaks at 1082, 1112 and 1148 cm^{-1} demonstrate the existence of the OH bondings, respectively, to γ-OH, δ-2-OH and δ-1-OH [25]. The broad peak about 2678 cm^{-1} is the fundamental OH stretching related to the hydrogen bonding with an O–H–O length of ~2.60 Å in the structure of the manganite [18]. The peak at 2082 cm^{-1} is interpreted as the combination of the OH stretching mode at 2678 cm^{-1} and the excited lattice mode at 594 cm^{-1}, that is, 2678 – 594 = 2084 cm^{-1}. This value is very close to that which Zhang *et al.* [26] have reported.

3.4. Influential factors on the formation of MnOOH nanorods: The nature of nanomaterials formed by the hydrothermal route depends on various factors such as the solvent used, temperature, reaction time, effective fill level in the pressure vessel and so forth [27]. The factors mentioned above can be judicially chosen to obtain the desired architectures. The morphology and dimensions of the samples were found to strongly depend on the mass ratios of PVP/$KMnO_4$, reaction time and reaction temperature. It is well known that a PVP molecule contains a carbonyl group, which makes PVP be a reducing agent, and $KMnO_4$ can be easily reduced by PVP to form manganese oxides with a lower valance state. The reducing ability of PVP would be affected by the PVP concentration (the PVP concentration is decreased with the decreasing of the mass ratio between PVP and$KMnO_4$). As we all know, manganese element exists in various valences from +2 to +7. So, by changing the PVP concentration to adjust the reducing ability of PVP, manganese-based compounds with different manganese valance states could be obtained. When the reaction was carried out at 160°C for 16 h, the morphologies of samples change from nanorods to nanoparticles with the decrease of the mass ratios of PVP/$KMnO_4$ as depicted in the SEM images (Fig. 4). MnOOH nanorods are the major products when the mass ratio is in the range of 2.0 – 0.3 (Figs. 2*a* and 4*a*–*c*). The as-synthesised MnOOH nanorods, typically 10 – 20 μm in length, have tetragonal cross-sections with edge lengths in the range of 100 – 400 nm, delivering unexpectedly high aspect ratios larger than 1000. Such a high aspect ratio of a one-dimensional nanostructure is uncommon in solution-based synthesis. MnO_2 nanoparticles could be obtained when the mass ratio was decreased to 0.1 (Fig. 4*d*). The inset in Fig. 4*d* shows the XRD pattern of the MnO_2 sample prepared under the mass ratio of 0.1 (the lower PVP concentration), which

doi: 10.1049/mnl.2013.0010

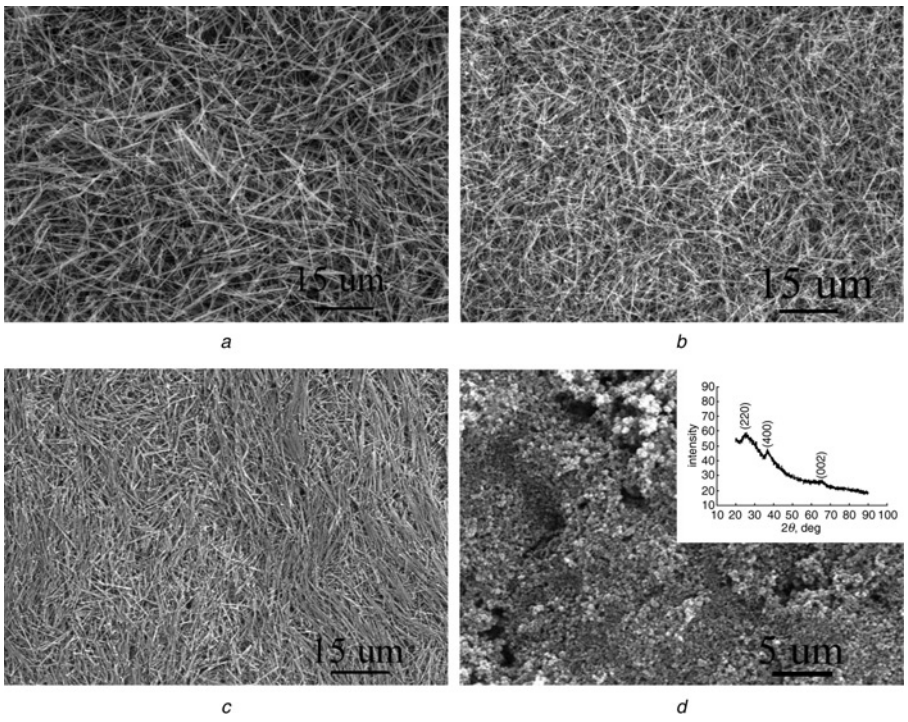

Figure 4 *SEM images of samples obtained at 160°C for 16 h with various mass ratios of PVP/$KMnO_4$*
Mass ratios of PVP/$KMnO_4$
a 1.0
b 0.5
c 0.3
d 0.1

can be indexed to α-MnO_2 (JCPDS No. 44-0141) [28]. MnOOH and MnO_2 are formed, indicating that manganese compounds with different oxidation states of +3 and +4 have been obtained, respectively.

Comparative experiments were carried out at other temperatures. Fig. 5*a* shows the SEM image of the sample prepared at 100°C. It can be observed that the sample consists of large quantities of small particles. Only a few nanorods are obtained as shown in Fig. 5*b* when the experiment was conducted at 120°C. When the temperatures were increased to 140 or 160°C, the products were dominated by nanorods (Figs. 5*c* and 2*a*). However, the morphology transforms to the mixture of nanorods and nanoparticles as shown in Fig. 5*d* at higher temperature (180°C). The above results indicate that suitable conditions are needed to obtain MnOOH nanorods. In general, a higher temperature is favourable for the reduction of $KMnO_4$. Here we chose 160°C as the synthetic temperature because the reaction can be completed more quickly.

To understand further the formation process of MnOOH nanorods, we carried out time-dependent experiments at 160°C (Fig. 6). At an early stage (3 h of hydrothermal reaction), the products were mainly composed of small nanoparticles, accompanying a few rod-like architectures (Fig. 6*a*). When the reaction time was prolonged to 12 h, the products were basically composed of MnOOH nanorods besides several nanoparticles (Fig. 6*b*). However, uniform MnOOH nanorods were obtained when the reaction time was raised to 16 h (Fig. 2*a*). It could be deduced that many

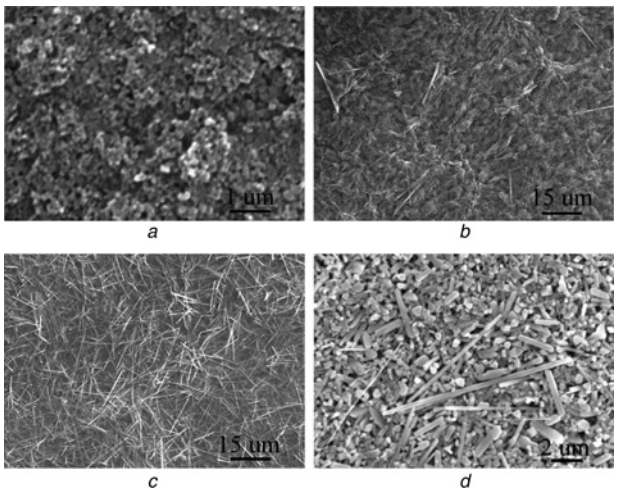

Figure 5 *SEM images of samples obtained with various temperatures*
Temperature (°C)
a 100
b 120
c 140
d 180

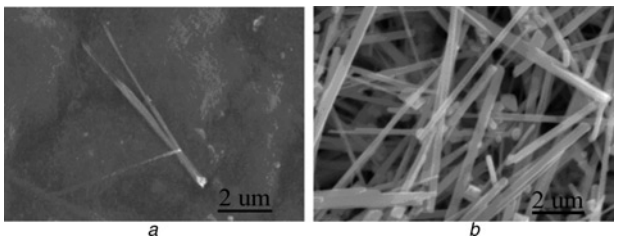

Figure 6 *SEM images of samples obtained at 160°C with different reaction time*
Mass ratio between PVP and $KMnO_4$: and reaction time (h)
a 3
b 12

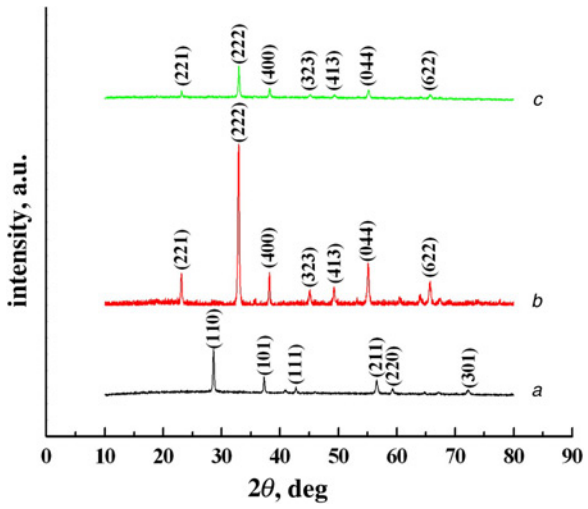

Figure 7 *XRD patterns of MnOOH nanorods after calcination at various temperatures*
Temperature (°C)
a 300
b 400
c 600

MnOOH nuclei form at the beginning of the reaction and as the reaction goes forward, MnOOH nanoparticles would grow to form rod-like architectures by Ostwald's ripening process [29]. In this process, PVP molecules should act not only as reactants but also as crystal growth modifiers [30]. PVP molecules in solution would have preferential absorption abilities to different crystal faces of MnOOH, which would affect the growth rates along different crystal axes during the Ostwald's ripening process and result in the growth of nanoparticles into MnOOH nanorods [31].

3.5. Morphology-conserved transformation from MnOOH nanorods to MnO_2 and Mn_2O_3 nanorods: The crystal structure of the samples prepared with different calcination temperatures was examined by XRD. Fig. 7 shows the XRD patterns of the samples produced by calcining MnOOH nanorods at various temperatures. MnOOH was transformed into MnO_2 when the calcination temperature was 300°C. The XRD pattern in Fig. 7*a* confirmed the formation of MnO_2 (JCPDS No. 24-0735) with no other crystalline phase. All the diffraction peaks in Figs. 7*b* and *c* can be readily indexed to the pure phase of Mn_2O_3 (JCPDS No. 24-0508) with lattice constants a = 9.4161 Å, b = 9.4237 Å, c = 9.4051 Å. The XRD results showed that Mn_2O_3 was obtained when the calcination temperature was raised to 400 or 600°C. The formation process of MnO_2 and Mn_2O_3 can be described as the following equations

$$4MnOOH + O_2 \xrightarrow{300^\circ C} 4MnO_2 + 2H_2O \quad (1)$$

$$4MnOOH \xrightarrow{400-600^\circ C} 2Mn_2O_3 + 2H_2O \quad (2)$$

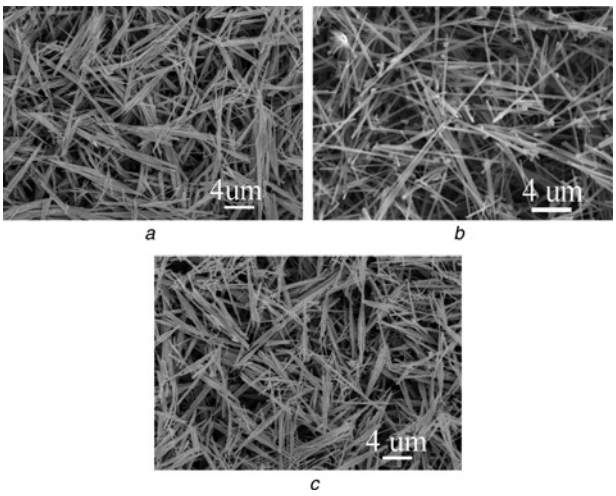

Figure 8 *SEM images of MnOOH nanorods after calcination at various temperatures*
Temperature (°C)
a 300
b 400
c 600

The morphologies of calcination samples prepared at various temperatures are depicted in Fig. 8. Compared with Figs. 2*a* and *b*, we can see that the morphologies of MnOOH nanorods were well reserved in the MnO_2 and Mn_2O_3 nanorods samples, and no obvious difference was observed.

4. Conclusion: Single crystal MnOOH nanorods with lengths up to 20 μm and diameters in the range of 100–400 nm have been synthesised on a large scale using a simple hydrothermal reaction between $KMnO_4$ and PVP. The formation mechanism was preliminarily discussed on the base of Ostwald's ripening process. In addition, uniform MnO_2 and Mn_2O_3 nanorods with high aspect ratios were produced facilely by calcination of MnOOH nanorods.

5. Acknowledgments: This work was supported by the University Natural Scientific Foundation of Jiangsu Province (grant no. 11KJB150003) and the Project for Jiangsu Province College student's Practice and Innovation.

6 References

[1] Devaraj S., Munichandraiah N.: 'Effect of crystallographic structure of MnO_2 on its electrochemical capacitance properties', *J. Phys. Chem. C*, 2008, **112**, pp. 4406–4417
[2] Feng Z.-P., Li G.-R., Zhong J.-H., *ET AL.*: 'MnO_2 multilayer nanosheet clusters evolved from monolayer nanosheets and their predominant electrochemical properties', *Electrochem. Commun.*, 2009, **11**, pp. 706–710
[3] Cao X., Wang N., Wang L., *ET AL.*: 'A novel non-enzymatic hydrogen peroxide biosensor based on ultralong manganite MnOOH nanowires', *Sens. Actuators B, Chem.*, 2010, **147**, pp. 730–734
[4] Li X., Zhou L., Gao J., *ET AL.*: 'Synthesis of Mn_3O_4 nanoparticles and their catalytic applications in hydrocarbon oxidation', *Powder Technol.*, 2009, **190**, pp. 324–326
[5] Zhao J., Tao Z., Liang J., *ET AL.*: 'Facile synthesis of nanoporous γ-MnO_2 structures and their application in rechargeable Li-ion batteries', *Cryst. Growth Des.*, 2008, **8**, pp. 2799–2805
[6] Yu P., Zhang X., Wang D., *ET AL.*: 'Shape-controlled synthesis of 3D hierarchical MnO_2 nanostructures for electrochemical supercapacitors', *Cryst. Growth Des.*, 2009, **9**, pp. 528–533
[7] Yang L.-X., Liang Y., Chen H., *ET AL.*: 'Controlled synthesis of Mn_3O_4 and $MnCO_3$ in a solvothermal system', *Mater. Res. Bull.*, 2009, **44**, pp. 1753–1759
[8] Wang X., Wang X., Huang W., *ET AL.*: 'Sol–gel template synthesis of highly ordered MnO_2 nanowire arrays', *J. Power Sources*, 2005, **140**, pp. 211–215
[9] Chang J.-K., Hsu S.-H., Tsai W.-T., *ET AL.*: 'A novel electrochemical process to prepare a high-porosity manganese oxide electrode with promising pseudocapacitive performance', *J. Power Sources*, 2008, **177**, pp. 676–680
[10] Askarinejad A., Morsali A.: 'Direct ultrasonic-assisted synthesis of sphere-like nanocrystals of spinel Co_3O_4 and Mn_3O_4', *Ultrason. Sonochem.*, 2009, **16**, pp. 124–131
[11] Salavati-Niasari M., Davar F., Mazaheri M.: 'Synthesis of Mn_3O_4 nanoparticles by thermal decomposition of a [bis(salicylidiminato) manganese(II)] complex', *Polyhedron*, 2008, **27**, pp. 3467–3471

doi: 10.1049/mnl.2013.0010

[12] Chang Y.Q., Yu D.P., Long Y., *ET AL.*: 'Large-scale fabrication of single-crystalline Mn_3O_4 nanowires via vapor phase growth', *J. Cryst. Growth*, 2005, **279**, pp. 88–92
[13] Apte S.K., Naik S.D., Sonawane R.S., *ET AL.*: 'Nanosize Mn_3O_4 (Hausmannite) by microwave irradiation method', *Mater. Res. Bull.*, 2006, **41**, pp. 647–654
[14] Chen S., Zhu J., Han Q., *ET AL.*: 'Shape-controlled synthesis of one-dimensional MnO_2 via a facile quick-precipitation procedure and its electrochemical properties', *Cryst. Growth Des.*, 2009, **9**, pp. 4356–4361
[15] Li Z., Xu J., Chen X., *ET AL.*: 'A simple hydrothermal route to synthesis of rod-like MnOOH and spindle-shaped $MnCO_3$', *Colloid Polym. Sci.*, 2011, **289**, pp. 1643–1651
[16] El-Deab M.S.: 'Electrocatalytic oxidation of methanol at γ-MnOOH nanorods modified Pt electrodes', *Int. J. Electrochem. Sci.*, 2009, **4**, pp. 1329–1338
[17] Li Z., Bao H., Miao X., *ET AL.*: 'A facile route to growth of γ-MnOOH nanorods and electrochemical capacitance properties', *J. Colloid Interface Sci.*, 2011, **357**, pp. 286–291
[18] Li F., Wu J., Qin Q., *ET AL.*: 'Facile synthesis of γ-MnOOH micro/nanorods and their conversion to B-MnO_2, Mn_3O_4', *J. Alloys Compd.*, 2010, **492**, pp. 339–346
[19] Zhou F., Zhao X., Yuan C., *ET AL.*: 'Synthesis of γ-MnOOH nanorods and their isomorphous transformation into β-MnO_2 and α-Mn_2O_3 nanorods', *J. Mater. Sci.*, 2007, **42**, pp. 9978–9982
[20] Cheng F., Shen J., Ji W., *ET AL.*: 'Selective synthesis of manganese oxide nanostructures for electrocatalytic oxygen reduction', *ACS Appl. Mater. Interfaces*, 2009, **1**, pp. 460–466
[21] Gao L., Fei L., Zheng H.: 'Preparation of α-MnO_2 nanowires through a γ-MnOOH precursor route', *Mater. Lett.*, 2007, **61**, pp. 1785–1788
[22] Zhang W., Wang H., Yang Z., *ET AL.*: 'Promotion of H_2O_2 decomposition activity over β-MnO_2 nanorod catalysts', *Colloid Surf. A*, 2007, **304**, pp. 60–66
[23] Wu Y.-T., Hu C.-C.: 'Aspect ratio controlled growth of mnooh in mixtures of Mn_3O_4 and MnOOH single crystals for supercapacitors', *Electrochem. Solid-State Lett.*, 2005, **8**, pp. A240–A244
[24] Ocaña M.: 'Uniform particles of manganese compounds obtained by forced hydrolysis of manganese(II) acetate', *Colloid Polym. Sci.*, 2000, **278**, pp. 443–449
[25] Zhang W., Yang Z., Liu Y., *ET AL.*: 'Controlled synthesis of Mn_3O_4 nanocrystallites and MnOOH nanorods by a solvothermal method', *J. Cryst. Growth*, 2004, **263**, pp. 394–399
[26] Zhang Y.C., Qiao T., Hu X.Y., *ET AL.*: 'Simple hydrothermal preparation of γ-MnOOH nanowires and their low-temperature thermal conversion to β-MnO_2 nanowires', *J. Cryst. Growth*, 2005, **280**, pp. 652–657
[27] Byrappa K., Adschiri T.: 'Hydrothermal technology for nanotechnology', *Prog. Cryst. Growth Charact.*, 2007, **53**, pp. 117–166
[28] Yang Y., Huang C.: 'Effect of synthetical conditions, morphology, and crystallographic structure of MnO_2 on its electrochemical behavior', *J. Solid State Electrochem.*, 2010, **14**, pp. 1293–1301
[29] Cushing B.L., Kolesnichenko V.L., O'Connor C.J.: 'Recent advances in the liquid-phase syntheses of inorganic nanoparticles', *Chem. Rev.*, 2004, **104**, pp. 3893–3946
[30] Zheng D., Yin Z., Zhang W., *ET AL.*: 'Novel branched γ-MnOOH and β-MnO_2 multipod nanostructures', *Cryst. Growth Des.*, 2006, **6**, pp. 1733–1735
[31] Murphy C.J.: 'Materials science: nanocubes and nanoboxes', *Science*, 2002, **298**, pp. 2139–2141